Design and Synthesis of TiO_2 Nanorod Assemblies and Their Application for Photovoltaic Devices

Qingshuo Wei,[†] Kouske Hirota,[†,‡] Keisuke Tajima,[†] and Kazuhito Hashimoto*[,†]

Department of Applied Chemistry, School of Engineering, The University of Tokyo, 7-3-1 Hongo, Bunkyo-ku, Tokyo 113-8656, Japan, and Electronic and Engineered Materials Laboratory, Mitsui Chemicals, Inc., 580-32 Nagaura, Sodegaura, Chiba 299-0265, Japan

Received July 20, 2006

We have developed a new method to fabricate an array of TiO_2 nanorod assemblies on a flat TiO_2 surface. The TiO_2 nanostructures with a height of approximately 40 nm were synthesized via a low temperature sol−gel reaction in a reversed micelle system. Cross-sectional transmission electron microscopy observation revealed that each nanostructure is an assembly of nanorods with a diameter and length of approximately 4 nm and approximately 40 nm, respectively. The fabricated array of TiO_2 nanorods was applied to construct photovoltaic devices combined with a semiconducting polymer. When the nanostructured TiO_2 substrate is used, photovoltaic performance reaches a power conversion efficiency of 0.39% and a fill factor of 0.47 under AM 1.5 illumination. Dependence of external quantum efficiency on polymer thickness showed the maximum efficiency in a thicker polymer film condition in the presence of the TiO_2 nanorod assembly, indicating the nanostructure functions as an efficient exciton collector.

Introduction

Photovoltaic devices based on conjugated polymers have been attracting much attention in the past decades, as a promising candidate for renewable resources of electrical energy.[1−3] Compared with conventional silicon solar cells, these devices are attractive because of their low production cost, flexibility, and possibility of large-area products. Recent research indicates that the device performances are very sensitive to nanostructures in active layers, which are known to greatly affect the charge separation and transportation in the semiconducting materials.[4−6] If we can construct intrinsic nanostructures in the active layer by material design, it could provide a methodology to further improve the device performance. A promising structure for the photovoltaic devices has been proposed to be an ordered interdigitating nanostructure of electron acceptor and donor, as shown in Figure 1.[7−11] In this structure, we could achieve both a large interface between the semiconducting materials and straight carrier paths to the electrodes. The structural dimension of less than 20 nm is desirable, because the diffusion length of excitons in a semiconducting polymer is smaller than 20 nm.[12−14]

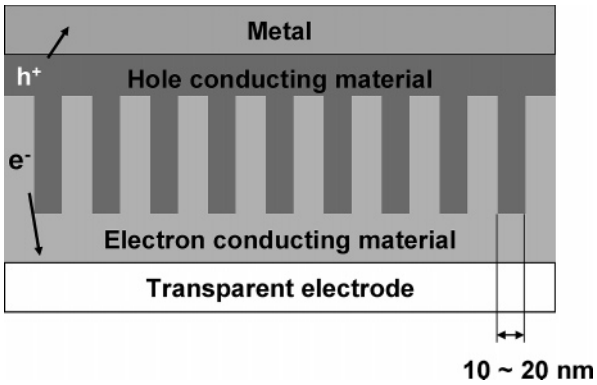

Figure 1. Schematic representation of a photovoltaic device with an "ideal" interdigitating nanostructure.

To achieve this type of nanostructure for photovoltaic application, inorganic semiconducting materials have an advantage because of their versatility and robustness of the structures. Titanium dioxide (TiO_2) is one of the best-studied inorganic materials for hybrid metal-oxide/polymer photovoltaic devices because of its electron accepting and conducting ability. In early studies, dense and flat layers of TiO_2 films were combined with semiconducting polymers to fabricate bilayer photovoltaic devices.[13−18] "Bulk-hetero-

* Corresponding author. Phone: +81-3-5841-7244. Fax: +81-3-5841-8751. E-mail: hashimoto@light.t.u-tokyo.ac.jp.
[†] The University of Tokyo.
[‡] Mitsui Chemicals, Inc.

(1) Yu, G.; Gao, J.; Hummelen, J. C.; Wudl, F.; Heeger, A. J. *Science* **1995**, *270*, 1789.
(2) Brabec, C. J.; Sariciftci, N. S.; Hummelen, J. C. *Adv. Funct. Mater.* **2001**, *11*, 15.
(3) Spanggaard, H.; Krebs, F. C. *Sol. Energy Mater. Sol. Cells* **2004**, *83*, 125.
(4) Shaheen, S. E.; Brabec, C. J.; Sariciftci, N. S.; Padinger, F.; Fromherz, T.; Hummelen, J. C. *Appl. Phys. Lett.* **2001**, *78*, 841.
(5) Ma, W. L.; Yang, C. Y.; Gong, X.; Lee, K.; Heeger, A. J. *Adv. Funct. Mater.* **2005**, *15*, 1617.
(6) Reyes-Reyes, M.; Kim, K.; Carroll, D. L. *Appl. Phys. Lett.* **2005**, *87*, 083506.
(7) Salafsky, J. S. *Solid-State Electron.* **2001**, *45*, 53.
(8) Kannan, B.; Castelino, K.; Majumdar, A. *Nano Lett.* **2003**, *3*, 1729.
(9) Coakley, K. M.; McGehee, M. D. *Chem. Mater.* **2004**, *16*, 4533.
(10) Coakley, K. M.; Liu, Y. X.; Goh, C.; McGehee, M. D. *MRS Bull.* **2005**, *30*, 37.
(11) Olson, D. C.; Piris, J.; Collins, R. T.; Shaheen, S. E.; Ginley, D. S. *Thin Solid Films* **2006**, *496*, 26.
(12) Friend, R. H.; Denton, G. J.; Halls, J. J. M.; Harrison, N. T.; Holmes, A. B.; Kohler, A.; Lux, A.; Moratti, S. C.; Pichler, K.; Tessler, N.; Towns, K.; Wittmann, H. F. *Solid State Commun.* **1997**, *102*, 249.
(13) Savenije, T. J.; Warman, J. M.; Goossens, A. *Chem. Phys. Lett.* **1998**, *287*, 148.
(14) Arango, A. C.; Johnson, L. R.; Bliznyuk, V. N.; Schlesinger, Z.; Carter, S. A.; Horhold, H. H. *Adv. Mater.* **2000**, *12*, 1689.

10.1021/cm061697b CCC: $33.50
Published on Web 09/21/2006

junction" devices using a mixture of a semiconducting polymer and TiO_2 nanocrystals or a precursor for TiO_2 were also reported.[19−25] Recently, hybrid photovoltaic devices were successfully fabricated by filling nanoporous TiO_2 films or a TiO_2 network with semiconducting polymers.[26−32] This is one method to achieve an interdigitating nanostructure shown in Figure 1. Another possibility to achieve this structure is to have vertically oriented nanorods of electron conducting materials covered with hole conducting polymers. In this way, it can be easier to make the polymer infiltrate into the nanostructured electron conducting materials, compared with nanoporous materials. Very recently, Olson et al. proposed using ZnO nanorods for realization of this type of structure.[11]

Herein we report synthesis of a novel TiO_2 nanostructure consisting of crystalline nanorods and its application to inorganic/polymer hybrid photovoltaic devices. The array of TiO_2 nanorod assemblies on the electrode surface is expected to provide a large interface for the charge separation and a straight pathway for electron transport to the electrode.

Experimental Section

Materials. Tetraisopropyl orthotitanate ($((CH_3)_2CHO)_4Ti$) and trimethylamine-*N*-oxide dihydrate ($(CH_3)_3NO{\cdot}2H_2O$ or TMAO, >98%) were purchased from Tokyo Kasei Kogyo. Oleic acid ($C_{18}H_{33}COOH$ or OLEA, 90%), poly[2-methoxy-5-(2′-ethylhexyloxy)-1,4-phenylenevinylene] ($(C_{18}H_{28}O_2)_n$ or MEH-PPV, average $M_n = 51\,000$), and chlorobenzene (C_6H_5Cl, 99.8%) were purchased from Aldrich. All the chemicals were used as received. Indium tin oxide (ITO)-coated glass was purchased from Kuramoto, Japan.

Preparation of Flat TiO_2 Films. A cleaned ITO/glass was dipped into a precursor solution (NDH-510C, Nippon Soda) and then pulled up at a constant rate (12 mm/min). After the coating, the substrate was dried at 120 °C for 0.5 h and then baked at 500 °C in the air for 0.5 h to convert the amorphous film to a crystalline film of anatase. The thickness of the film was around 50 nm.

Synthesis of TiO_2 Nanostructures. The precursor solution for TiO_2 was prepared according to the method of Cozzoli et al.[33] A total of 40 mL of OLEA was placed in a 50 mL two-neck flask and connected to a vacuum to dehydrate at 90 °C for 1 h. A total of 1.5 mL of tetraisopropyl orthotitanate was added under a nitrogen atmosphere and stirred at 90 °C for 5 min. When the solution turned to pale yellow, 0.75 g of TMAO was added. After the TMAO dissolved in the solution, 5 mL of the solution was taken into a 15 mL PFA container where the substrate was already set with the ITO side facing up. A total of 0.6 mL of water was injected into the PFA container and aged at 90 °C for 12 h. After being aged in the oven, the substrate was carefully washed first by rinsing with hexane for several times and then by immersing it into hexane for several hours. After the substrate was dried, it was heated at 500 °C for 0.5 h to remove the residual organic compounds such as OLEA.

Preparation of Photovoltaic Devices. A chlorobenzene solution of MEH-PPV was spin-coated on the TiO_2 substrates and annealed under a vacuum at 100 °C for 10 min. The thickness of the polymer layer was controlled both by the speed used in the spin-coating and by the concentration of the polymer solution. Au electrodes were then evaporated under high vacuum (lower than 1×10^{-3} Pa) in the ULVAC UPC-260F vacuum evaporation system at 0.1 nm/s. The thickness of the gold is around 100 nm. Copper wires and silver paste were used to connect the two electrodes. The active area of each device is 2 mm × 3 mm.

Polymer Thickness. To determine the polymer thickness, an interference fringe at a low angle from X-ray diffraction was used for the films deposited on glass substrates. UV−vis absorbance of the films was measured to determine the absorption coefficient. A linear relationship between the absorbance and the polymer thickness was obtained. The absorption coefficient of $\epsilon = 7.6 \times 10^4$ cm^{-1} at $\lambda = 510$ nm was obtained for the MEH-PPV film, which is close to the value reported of $\epsilon = 9 \times 10^4$ cm^{-1}.[15]

Characterization. Atomic force microscopy (AFM) measurement was carried out on Digital Instrumental Nanoscope 31 operated in the tapping mode. Micro-fabricated silicon cantilevers with a spring constant of 32 N m^{-1} were used. Field-emission scanning electron microscopy (FE-SEM) was performed on a Hitachi S-900 with an accelerating voltage of 10 kV. Transmission electron microscopy (TEM) studies were carried out on a JEM-4000EX II electron microscope operated at 400 kV. Samples for TEM cross-sectional observation were prepared first by wrapping with epoxy resin and then by thinning using microtome and ion milling.

Photovoltaic Measurement. The current−voltage characteristics of the photovoltaic devices were measured with the Agilent Technologies E5273A C-V measurement system. For EQE measurement, a HAYASHI LA-210UV xenon lamp and JASCO CT-25CP grating monochromator were used. The power conversion efficiency (PCE) was examined with the USHIO SX-UID501CMQ xenon lamp with an AM 1.5 filter. The light intensity was adjusted by a standard silicon solar cell (Bunkou Keiki BS520) in the wavelength range of 300−1200 nm.

Results and Discussion

Preparation of TiO_2 Nanostructures. Cozzoli et al. developed a method for a low temperature sol−gel synthesis of anatase TiO_2 nanorods in a reversed micelle solution.[33]

(15) Breeze, A. J.; Schlesinger, Z.; Carter, S. A.; Brock, P. J. *Phys. Rev. B* **2001**, *64*, 125205.
(16) Fan, Q.; McQuillin, B.; Bradley, D. D. C.; Whitelegg, S.; Seddon, A. B. *Chem. Phys. Lett.* **2001**, *347*, 325.
(17) Grant, C. D.; Schwartzberg, A. M.; Smestad, G. P.; Kowalik, J.; Tolbert, L. M.; Zhang, J. Z. *J. Electroanal. Chem.* **2002**, *522*, 40.
(18) Liu, J. S.; Kadnikova, E. N.; Liu, Y. X.; McGehee, M. D.; Frechet, J. M. J. *J. Am. Chem. Soc.* **2004**, *126*, 9486.
(19) Salafsky, J. S. *Phys. Rev. B* **1999**, *59*, 10885.
(20) van Hal, P. A.; Wienk, M. M.; Kroon, J. M.; Verhees, W. J. H.; Slooff, L. H.; van Gennip, W. J. H.; Jonkheijm, P.; Janssen, R. A. J. *Adv. Mater.* **2003**, *15*, 118.
(21) Kwong, C. Y.; Choy, W. C. H.; Djurisic, A. B.; Chui, P. C.; Cheng, K. W.; Chan, W. K. *Nanotechnology* **2004**, *15*, 1156.
(22) Kwong, C. Y.; Djurisic, A. B.; Chui, P. C.; Cheng, K. W.; Chan, W. K. *Chem. Phys. Lett.* **2004**, *384*, 372.
(23) Petrella, A.; Tamborra, M.; Cozzoli, P. D.; Curri, M. L.; Striccoli, M.; Cosma, P.; Farinola, G. M.; Babudri, E.; Naso, F.; Agostiano, A. *Thin Solid Films* **2004**, *451−452*, 64.
(24) Slooff, L. H.; Wienk, M. M.; Kroon, J. M. *Thin Solid Films* **2004**, *451−52*, 634.
(25) Slooff, L. H.; Kroon, J. M.; Loos, J.; Koetse, M. M.; Sweelssen, J. *Adv. Funct. Mater.* **2005**, *15*, 689.
(26) Coakley, K. M.; Liu, Y. X.; McGehee, M. D.; Frindell, K. L.; Stucky, G. D. *Adv. Funct. Mater.* **2003**, *13*, 301.
(27) Coakley, K. M.; McGehee, M. D. *Appl. Phys. Lett.* **2003**, *83*, 3380.
(28) Ravirajan, P.; Haque, S. A.; Poplavskyy, D.; Durrant, J. R.; Bradley, D. D. C.; Nelson, J. *Thin Solid Films* **2004**, *451−452*, 624.
(29) Ravirajan, P.; Haque, S. A.; Durrant, J. R.; Poplavskyy, D.; Bradley, D. D. C.; Nelson, J. *J. Appl. Phys.* **2004**, *95*, 1473.
(30) Ravirajan, P.; Bradley, D. D. C.; Nelson, J.; Haque, S. A.; Durrant, J. R.; Smit, H. J. P.; Kroon, J. M. *Appl. Phys. Lett.* **2005**, *86*, 143101.
(31) Ravirajan, P.; Haque, S. A.; Durrant, J. R.; Bradley, D. D. C.; Nelson, J. *Adv. Funct. Mater.* **2005**, *15*, 609.
(32) Wang, H.; Oey, C. C.; Djurisic, A. B.; Xie, M. H.; Leung, Y. H.; Man, K. K. Y.; Chan, W. K.; Pandey, A.; Nunzi, J. M.; Chui, P. C. *Appl. Phys. Lett.* **2005**, *87*, 023507.
(33) Cozzoli, P. D.; Kornowski, A.; Weller, H. *J. Am. Chem. Soc.* **2003**, *125*, 14539.

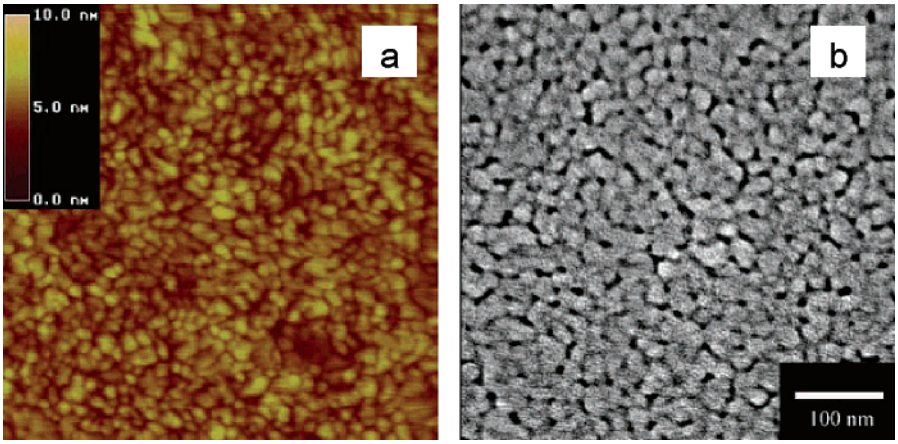

Figure 2. (a) AFM height image (image size, 500 nm × 500 nm; scan rate, 1.0 Hz; number of scan lines, 256) and (b) FE-SEM image of a flat TiO_2 substrate prepared by dip-coating.

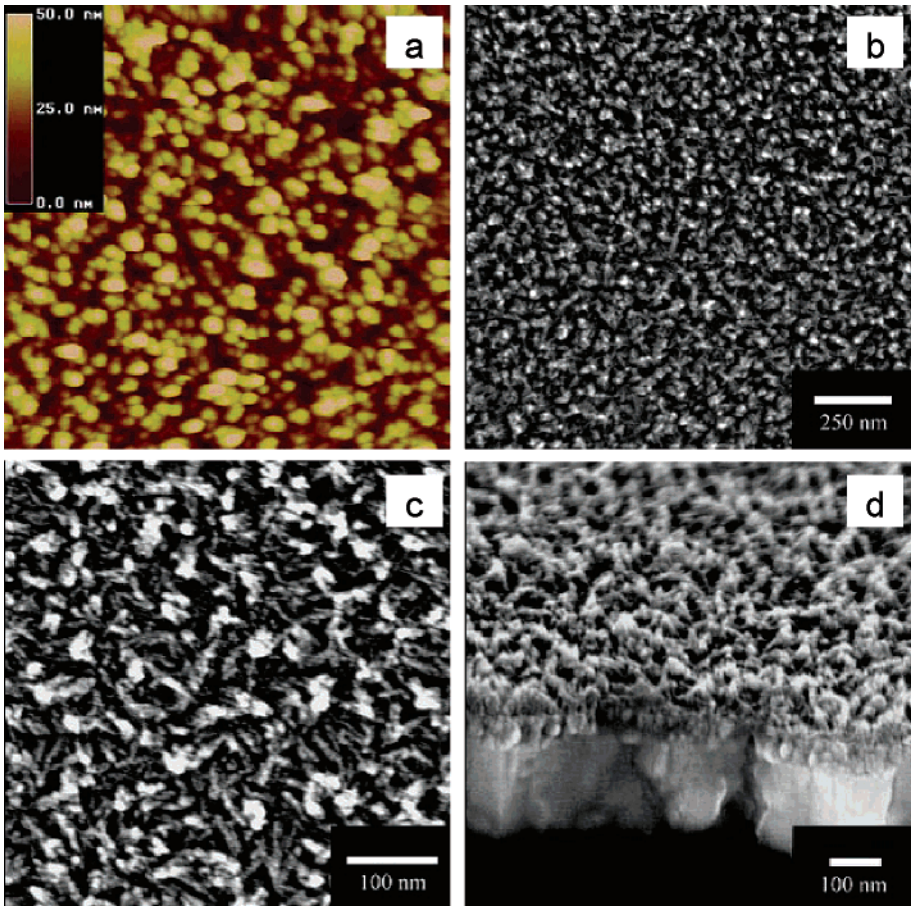

Figure 3. (a) AFM height image (image size, 1 μm × 1 μm; scan rate, 1.0 Hz; number of scan lines, 256) and (b−d) FE-SEM images of the TiO_2 nanostructures (b) with a low magnification, (c) with a high magnification, and (d) with a tilted configuration.

They reported that the TiO_2 nanorods formed in the solution have a high crystallinity and a high aspect ratio with the length of up to 40 nm. On the basis of this report, by introducing a flat TiO_2 substrate in the reversed micelle solution, we succeeded in depositing an array of TiO_2 nanorod assemblies selectively on the TiO_2 surface.

First, a thin layer of TiO_2 was prepared on an ITO/glass substrate by dip-coating followed by calcination at 500 °C. The morphology of the dip-coated TiO_2 substrate was examined by AFM and FE-SEM. Both the AFM height image (Figure 2a) and the FE-SEM image (Figure 2b) show a very flat surface with roughness of less than 5 nm.

For preparation of nanostructured TiO_2, the flat TiO_2 film deposited on an ITO substrate was immersed into a reversed micelle solution and was kept at 90 °C. AFM observation after 12 h of the immersion revealed that the surface became much rougher, with the vertical height difference of over 40 nm (Figure 3a). From an FE-SEM image at a low magnification (Figure 3b), we can see that the substrate surface is uniformly covered with an array of nanostructures over the area of at least several square micrometers without any defects. The size of each nanostructure is approximately 20 nm, and the distance between them is 20−50 nm. X-ray photoelectron spectroscopy (XPS) spectra of the surface

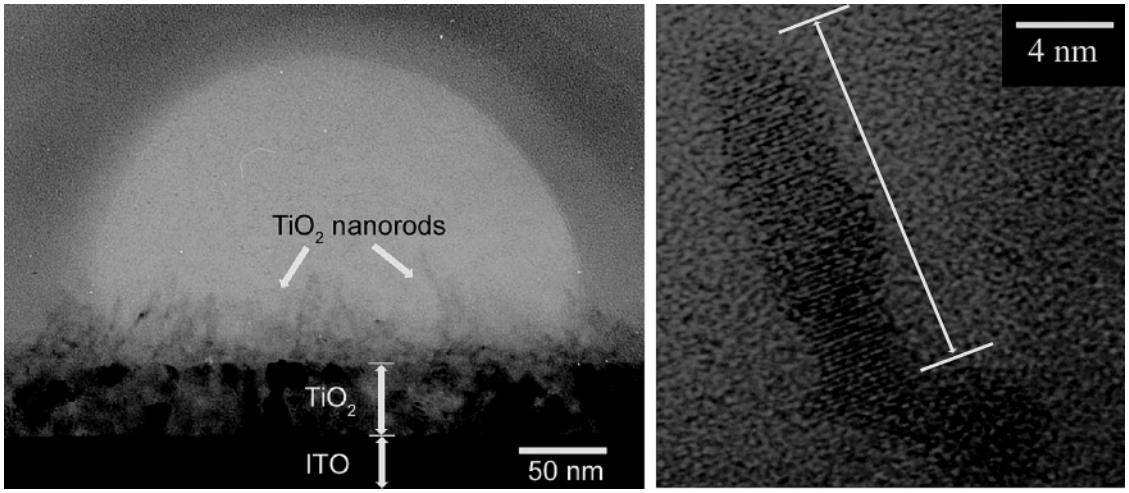

Figure 4. (a) TEM cross-sectional image of the nanostructured TiO_2 substrate and (b) high-resolution TEM lattice image of the TiO_2 nanorod.

exhibited a peak at 459 eV, corresponding to Ti 2p in TiO_2. This result indicates that those nanostructures are composed of TiO_2. A top view of the substrate by FE-SEM with a high magnification (Figure 3c) shows that each nanostructure is a secondary structure consisting of rod-shaped materials with diameters of several nanometers. Those rod-shaped materials can also be seen between the assemblies as white lines in Fiugre 3c. A tilted view of the nanostructured TiO_2 substrate by FE-SEM (Figure 3d) distinctly shows four layers, that is, from the bottom as follows: glass substrate, ITO film, flat TiO_2 film, and the array of TiO_2 nanostructures. The thickness of the TiO_2 nanostructured layer is estimated as around 40 nm from the image. Although the TiO_2 nanostructure is protruding from the surface, the orientation of the individual TiO_2 nanorods is not completely vertical, probably reflecting the multi-crystalline nature of the flat TiO_2 layer underneath.

To get a closer view of the array of the nanostructures, cross-sectional TEM observation was carried out. A TEM image in Figure 4a clearly shows the layers of the ITO, the flat TiO_2, and the array of the TiO_2 nanostructures, similar to the FE-SEM image. The vertical height of the nanostructure is around 40 nm, which coincides with the results of the AFM and FE-SEM observation. In the top layer, it is clearly observed that the TiO_2 nanostructures consist of nanorods as black lines, which seem directly attached to the flat layer of the TiO_2 substrate. Another TEM cross-sectional image with a higher magnification is given in Supporting Information. The nanorod feature is less clear in the region close to the substrate in the TEM image because several nanorods were overlapping (the diameters of the nanorods are 3−4 nm, and the sample thickness for TEM is around 50 nm). A blow-up of the higher magnification image (Figure 4b) shows that each TiO_2 nanorod consists of anisotropic single crystal domains with length and width of 10−20 nm and 3−4 nm, respectively.[34] The total length of each nanorod is approximately 40 nm. The shape of the nanorod on the surface is similar to the anatase TiO_2 nanorods formed in the solution under the same condition as reported in Cozzoli et al.'s paper. Combined with the high magnification FE-SEM image in Figure 3b, we conclude that each nanostructure is an assembly of crystalline TiO_2 nanorods.

(34) The background amorphous pattern comes from the epoxy resin that we used for the TEM sample preparation.

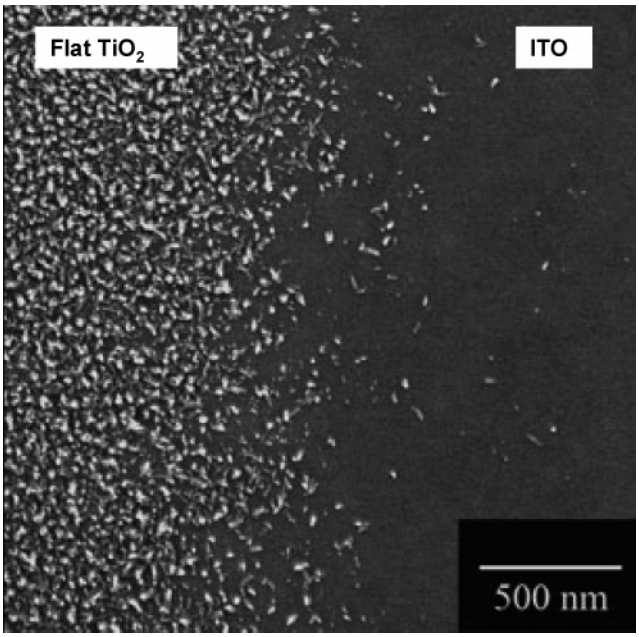

Figure 5. FE-SEM image of the border region between the dip-coated flat TiO_2 film (on the left) and the ITO substrate (on the right) after the growth of the TiO_2 nanostructure.

We found that formation of the array of TiO_2 nanorod assemblies occurs selectively on the TiO_2 film. A FE-SEM image of a border region between the flat TiO_2 film and the ITO substrate shows selective formation of the TiO_2 nanostructures only on the TiO_2 region, not on the ITO region (Figure 5). We have used different kinds of substrates such as ITO, glass, and silicon immersed in the solution under the same condition. No formation of the nanostructures was confirmed with the use of AFM and XPS. This indicates that the formation of the TiO_2 nanostructures is characteristic of the TiO_2 substrates. From this observation we can assume the formation mechanism of the TiO_2 nanorod assemblies: first the flat TiO_2 substrate functions as seeds for the TiO_2 nanorods, and then growth of the nanorods proceeds from the surface. The formation of rod-shaped material can be explained by the anisotropic reactivity of the titanium

precursor on different crystal surfaces of TiO_2 induced by inhibiting the effect of OLEA as previously reported.[33] The formation of the nanorod assemblies with the size of around 20 nm might be understood as a result of microscopic fluctuation in the concentration of the precursor near the surface. The TiO_2 nanorod assemblies are strongly attached on the flat TiO_2 substrate. Those structures cannot be removed when washed with water or an organic solvent such as hexane or even under sonication for several minutes. The selective formation and the strong attachment of the nanostructure on the TiO_2 substrate strongly support the growth of the TiO_2 nanorods from the TiO_2 surface and exclude the possibility of deposition of the nanorods formed in the solution. Further investigation such as using a single crystalline TiO_2 substrate could give us more information on the formation mechanism.

Photovoltaic Device Based on TiO_2 Nanostructure. In the previous section, we reported a successful preparation of an array of TiO_2 nanorod assemblies on flat TiO_2 substrates. We consider that the size, the spacing, and the crystalline nature of the TiO_2 nanostructures are suitable for use in photovoltaic devices. A large surface area of the nanorod assembly can contribute to an efficient exciton collection. These structures are projected from the flat TiO_2 substrate, which could provide direct pathways for electron transport.

For device preparation, ′MEH-PPV was used as an electron donor in all experiments. The polymer solution in chlorobenzene was spin-coated on the TiO_2/ITO substrates. The polymer thickness was controlled by changing the spin-coating conditions and the concentration of the MEH-PPV solution. We estimated the average thickness (i.e., quantity) of the polymer from the absorbance at 510 nm, because it was rather difficult to evaluate the actual thickness of the polymer film directly either from TEM, SEM, or AFM images because of the rough surface of the nanostructured TiO_2. After the films were annealed at 100 °C under vacuum for 10 min, gold electrodes were vacuum deposited on the polymer films to fabricate photovoltaic devices.

To elucidate the structure of the hybrid film, a FE-SEM cross-section image was taken for the polymer/nanostructured TiO_2 films (Figure 6). The film was annealed under the same conditions as those in the device preparation. No void was observed between the polymer and the nanostructure TiO_2, indicating that the polymer filled the interspaces between the TiO_2 nanorod assemblies. The relatively rough morphology of the surface is also considered to be the result of infiltration of the polymer into the indented structure of the TiO_2 nanorod assemblies. The infiltration of the polymer was further supported by fluorescence quenching measurement (see Supporting Information). Enhanced quenching of fluorescence from MEH-PPV was observed after thermal annealing under vacuum, indicating that the thermal annealing enlarged the interface between the polymer and TiO_2. Thus we conclude that the polymer can fill the interspaces between the TiO_2 nanorod assemblies, though it is not clear from the image whether the polymer filled the voids between the individual TiO_2 nanorods or not.

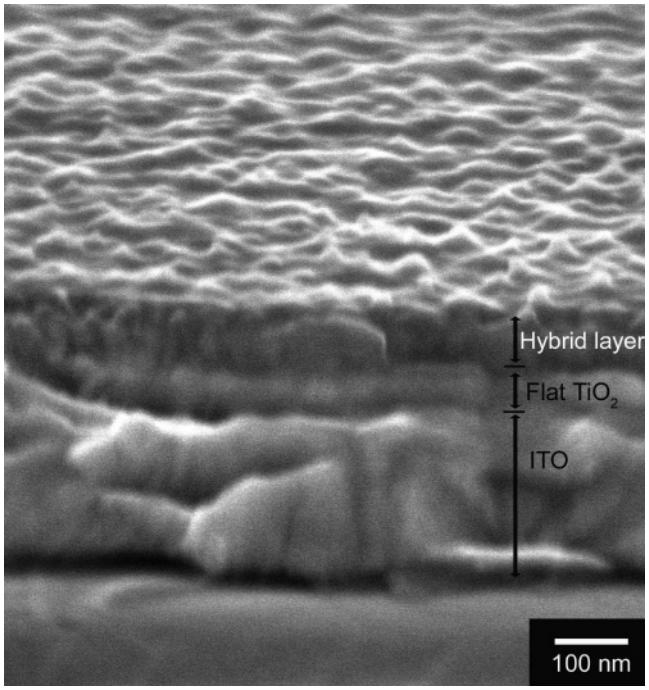

Figure 6. FE-SEM cross-sectional images of the MEH-PPV films deposited on the nanostructured TiO_2 substrates.

The surface morphology of the polymer films on the nanostructured TiO_2 after the annealing was characterized by AFM. Figure 7 shows the height images of the polymer films with different thicknesses. Along with the increase of polymer thickness (from part a to part c of Figure 7), the roughness of the film becomes smaller (roughness factors R_a for Figure 7a−c are 6.2, 4.8, and 2.8 nm, respectively), which is a reasonable result because the polymer can be easily filled in the interspaces of nanorod assemblies as described above. It is noteworthy that the devices can be successfully fabricated with good reproducibility showing no short circuits, even when the polymer thickness (8 nm estimated from absorption coefficient of the polymer film) is much smaller than the height of the nanostructure (ca. 40 nm).[35] This indicates that the polymer layer covers the nanostructures completely and that the gold electrode evaporated on the polymer surface does not touch these TiO_2 nanostructures directly. The low evaporation rate of gold (0.1 nm/s) seems to help to prevent the shorting problems as well.

Typical $I-V$ characteristics of the devices with the flat and nanostructured TiO_2 substrates are presented in Figure 8. Polymer thicknesses for the devices were optimized to achieve the highest efficiency (see below). Under the irradiation of 100 mW/cm^2 simulated solar light (AM 1.5), the device with the flat TiO_2 showed a short circuit current density (I_{sc}) of 0.33 mA/cm^2, an open circuit voltage (V_{oc}) of 0.87 V, and a fill factor (FF) of 0.49, resulting in a PCE

(35) Polymer thickness is determined by measuring the absorbance using the $\epsilon = 7.6 \times 10^4$ cm^{-1} at $\lambda = 510$ nm (see Experimental Section). For the nanostructured TiO_2 substrate, we have considered the volume effect of the TiO_2. The density of the nanorod assemblies is roughly estimated through the FE-SEM image to be 200 μm^{-2}, and the volume occupied by the nanostructures is estimated to be around 20%, leading to 45 nm thickness when the absorbance of the film is 0.26. The thickness of the active layer was also confirmed by FE-SEM cross-sectional images.

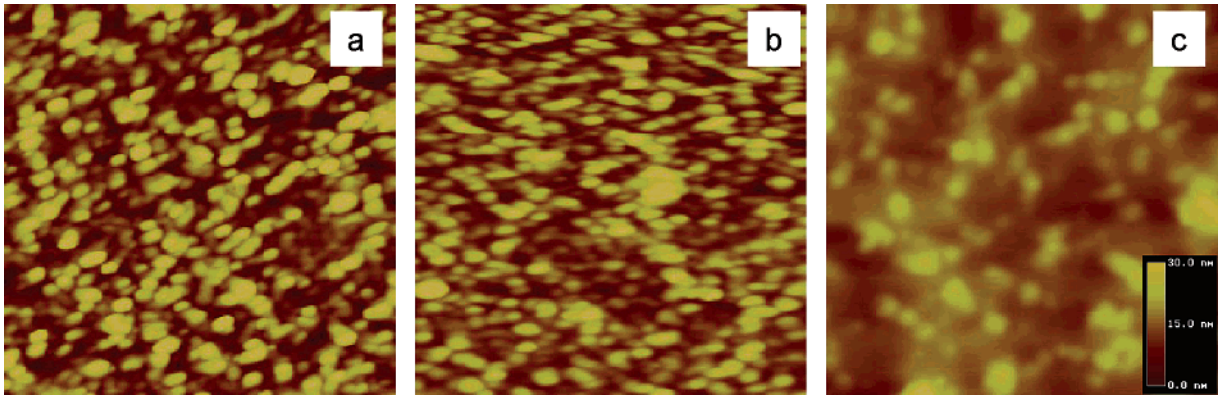

Figure 7. AFM height images of the MEH-PPV films deposited on the nanostructured TiO_2 substrates with different polymer thicknesses (image size, 1 μm $\times$ 1 μm; scan rate, 1.2 Hz; number of scan samples, 256). Absorbances of the active layer at 510 nm are (a) 0.06, (b) 0.21, and (c) 0.33, respectively.

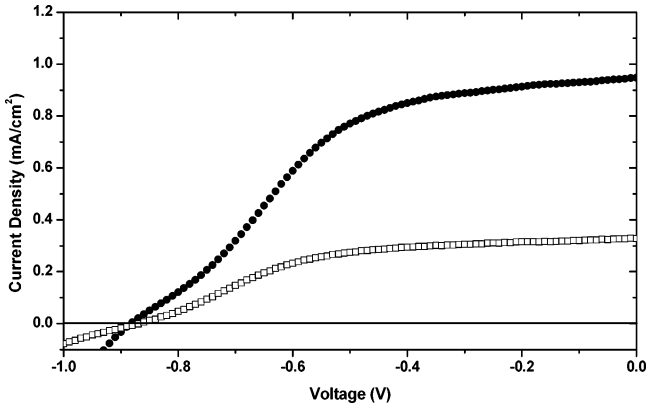

Figure 8. Current density−voltage curve of the MEH-PPV/TiO_2 photovoltaic devices under 100 mW/cm^2 AM 1.5 irradiation: devices with the nanostructured TiO_2 substrate (closed circles) and with the flat TiO_2 substrate (open squares).

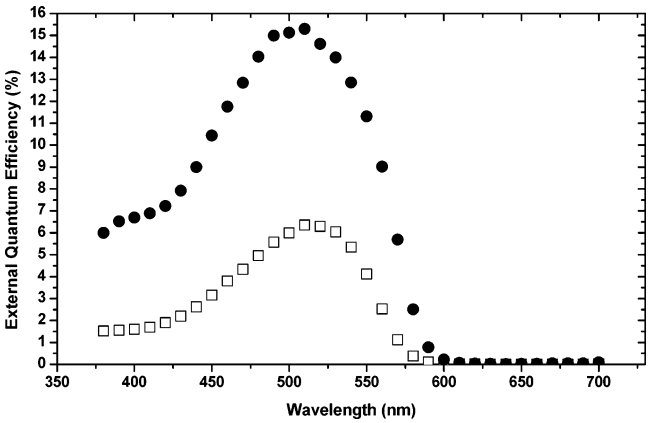

Figure 9. EQE plotted as a function of wavelength: devices with the nanostructured TiO_2 (closed circles) and with the flat TiO_2 (open squares).

of 0.14%. When the nanostructured TiO_2 substrate was used, a considerable improvement of the PCE up to 0.39% was observed with I_{sc} of 0.95 mA/cm^2, V_{oc} of 0.88 V, and FF of 0.47. External quantum efficiencies (EQEs) of the devices under monochromatic light are plotted as a function of wavelength (Figure 9). The maximum value of EQE for the nanostructured TiO_2 device reached 15% at 510 nm, which is close to a threefold improvement compared with the devices with the flat TiO_2. It is important to note that the introduction of the array of TiO_2 nanorod assemblies does

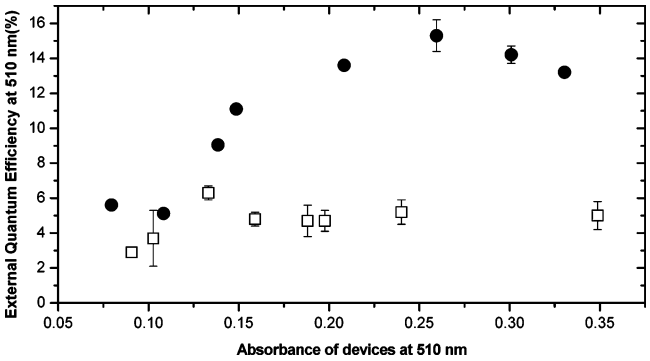

Figure 10. EQE dependence on polymer thickness: devices with the nanostructured TiO_2 substrates (closed circles) and with the flat TiO_2 substrates (open squares).

not lower the FF of the device. Under monochromatic light (510 nm, 0.2 mW/cm^2), the FF for the device with the TiO_2 nanostructures reached as high as 0.64. This value is again comparable with the device with flat TiO_2 (0.60 under the same condition) and with the highest value reported on bilayer devices using the crystallite TiO_2 substrate and MEH-PPV (0.67, EQE of 9.5% under the same light intensity at 500 nm).[16] Such a high FF of the device with the TiO_2 nanostructures could be explained by the effective electron transport within the TiO_2 nanorods, because of their single crystalline nature and good connection with the flat TiO_2 layer. We could observe small shoulders in $I-V$ curves for the devices both with the flat TiO_2 and with the nanostructured TiO_2, which deviate from the normal behaviors of organic solar cells. We consider that these shoulders could be caused by the increase of resistivity of ITO substrates, as the result of heating at 500 °C.

To further investigate photovoltaic performances of the devices with the TiO_2 nanostructures, the effect of the polymer thickness on EQEs was examined. Figure 10 shows EQEs under monochromatic light irradiation (510 nm), plotted as a function of polymer absorbance of the device. The EQEs of the devices with the nanostructured TiO_2 monotonously increased up to 15%, as the absorbance (i.e., the polymer thickness) was increased up to 0.26. Although the devices with the flat TiO_2 substrates showed a similar trend, the maximum EQE was only 6%, and it was observed at the absorbance of 0.13, corresponding to a much thinner polymer layer.

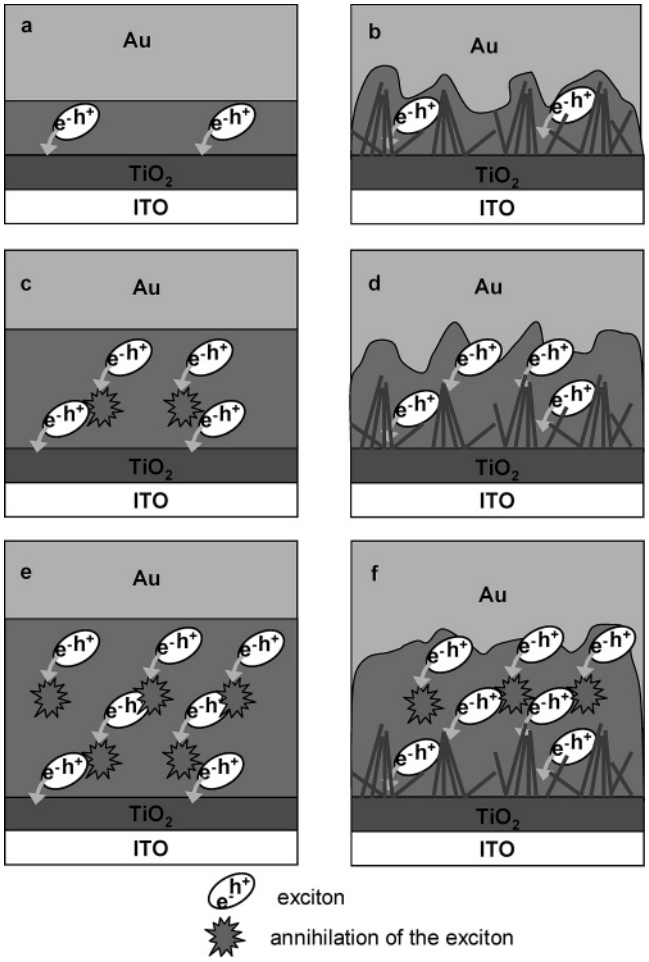

Figure 11. Schematic images of device structures (a, c, e) without and (b, d, f) with the nanostructured TiO_2 for different thicknesses of polymer: (a, b) when the polymer layer is very thin, (c, d) when the polymer thickness is increased, and (e, f) when the polymer layer is too thick. See the main text for details.

The EQE dependence on the polymer thickness shown in Figure 10 could be explained by more efficient exciton collection in the nanostructured TiO_2 devices. The situations with the different polymer thicknesses are schematically illustrated in Figure 11. With a thin layer of the polymer (Figure 11a,b), most of the generated excitons can diffuse to the interface between TiO_2 and MEH-PPV. Thus, the EQE increases as the number of the excitons generated increases, along with the absorbance of the film (i.e., the number of photons absorbed). In the device with a flat TiO_2 substrate, the thickness of the polymer film at the optimum condition (the absorbance of 0.13) was estimated as 18 nm by the absorption coefficient of the polymer.[35] This value coincides with the previous report on the fluorescence quenching dependence on the MEH-PPV thickness on flat TiO_2 substrates.[13]

In the region with higher absorbance, the EQE of devices with the flat TiO_2 decreased (Figure 11c). In contrast, with the device using the nanostructured TiO_2, the EQE continues to increase even when the thickness of the active layer exceeds the optimum polymer thickness on the flat TiO_2. This is probably because the excitons generated in between the nanorod assemblies contribute to the current, and thus the projecting structure of the TiO_2 substrate functions as an effective collector of the excitons. The thickness of the active layer at the optimum condition with absorbance of 0.26 was estimated as around 45 nm.[35] Under this condition, the surface roughness is small and the polymer infiltrated into the interspaces of the TiO_2 nanorod assemblies as schematically shown in Figure 11d.

When the polymer thickness exceeds the optimum value (Figure 11e,f), the EQE starts decreasing gradually. This phenomenon might be attributed to several factors. First, when the polymer layer is thicker, the contribution from the light reflected from the back electrode could be reduced, and thus the number of the excitons that contribute to photocurrent could decrease. Another factor is that holes generated at the TiO_2/polymer interface must go through the polymer layer to reach the Au electrode. A thicker polymer layer could cause more traps for the holes, so the number of collected charges could be reduced. Also, space-charge limited transport might occur when the polymer layer gets thicker because of the unbalanced charge mobility between the hole and the electron in the active layer.

The results of the EQE dependence on polymer thickness clearly demonstrate that the TiO_2 nanostructures have advantages in the exciton collection, leading to the high performance of the devices. Considering both the high FF and the improved EQEs deriving from the crystalline nature of TiO_2 and the effective collection of excitons, we conclude that the TiO_2 nanostructure achieved in this report is a promising candidate for realizing the ideal device structure shown in Figure 1. Further improvement of the photovoltaic performance could be achieved by optimization of the TiO_2 nanostructure. The distance within the TiO_2 nanostructure in our system (20−50 nm) might be larger than the optimum value, in consideration of the exciton diffusion length in the polymer (5−20 nm).[13,36−39] The short circuit current could be increased if the nanorods protrude individually and distribute uniformly on the surface, so the interface between TiO_2 and the polymer is increased. Also the elongation of the TiO_2 nanorods could enable us to fabricate devices with thicker polymer films without the loss of the generated charge carriers.

Conclusion

We have developed a new method to fabricate an array of TiO_2 nanorod assemblies on a flat TiO_2 surface. The TiO_2 nanorod assemblies function as an efficient exciton collector in polymer photovoltaic devices, resulting in improved PCE with a relatively high fill factor. Further optimization of this system could realize an ideal interdigitating structure suitable for high performance photovoltaic devices.

Acknowledgment. This work was supported by a Grant-in-Aid for Scientific Research on Priority Areas (Grant 417)

(36) Stubinger, T.; Brutting, W. *J. Appl. Phys.* **2001**, *90*, 3632.
(37) Markov, D. E.; Tanase, C.; Blom, P. W. M.; Wildeman, J. *Phys. Rev. B* **2005**, *72*, 045217.
(38) Markov, D. E.; Amsterdam, E.; Blom, P. W. M.; Sieval, A. B.; Hummelen, J. C. *J. Phys. Chem. A* **2005**, *109*, 5266.
(39) Halls, J. J. M.; Pichler, K.; Friend, R. H.; Moratti, S. C.; Holmes, A. B. *Appl. Phys. Lett.* **1996**, *68*, 3120.

from the Ministry of Education, Culture, Sports, Science, and Technology (MEXT) of the Japanese Government and partly by Nissan Science Foundation. We thank Messrs. T. Itoh, K. Ibe, and H. Tsunakawa (Institute of Engineering Innovation, School of Engineering, The University of Tokyo) for the TEM measurements and helpful discussion.

Supporting Information Available: TEM cross-sectional image of the nanostructured TiO_2 substrate and fluorescence quenching measurement details and plot for MEH-PPV (PDF). This material is available free of charge via the Internet at http://pubs.acs.org.

CM061697B